

Non-perturbative Effect and PAMELA Limit on Electro-Weak Dark Matter

Eung Jin Chun and Jong-Chul Park

*Korea Institute for Advanced Study
Heogiro 87, Dongdaemun-gu
Seoul 130-722, Korea
Emails: ejchun@kias.re.kr, jcpark@kias.re.kr*

Stefano Scopel

*Department of Physics, Sogang University
1 Sinsu-dong, Mapo-gu
Seoul 121-742, Korea
Email: scopel@sogang.ac.kr*

ABSTRACT: We discuss the non-perturbative effects on the annihilation cross section of an Electro-Weak Dark Matter (EWDM) particle belonging to an electroweak multiplet when the splittings between the masses of the DM component and the other charged or neutral component(s) of the multiplet are treated as free parameters. Our analysis shows that EWDM exhibits not only the usual Sommerfeld enhancement with resonance peaks but also dips where the cross section is suppressed. Moreover, we have shown that the non-perturbative effects become important even when the EWDM mass is below the TeV scale, provided that some of the mass splitting are reduced to the order of a few MeV. This extends the possibility of observing sizeable non-perturbative effects in the dark matter annihilation to values of the dark matter mass significantly smaller than previously considered, since only electroweak-induced mass splittings larger than 100 MeV have been discussed in the literature so far. We have then used the available experimental data on the cosmic antiproton flux to constrain the EWDM parameter space. In our calculation of the expected signal we have included the effect of the convolution of the cross section with the velocity distribution of the dark matter particles in the Galaxy, showing that it can alter the non-perturbative effects significantly. In the case of EWDM with non-zero hypercharge, we have shown that the mass splitting in the Dirac dark matter fermion can be chosen so that the inelastic cross section of the EWDM off nuclei is allowed by present direct detection constraints and at the same time is within the reach of future experiments.

KEYWORDS: Dark Matter, Sommerfeld effect, Ramsauer-Townsend effect.

Contents

1. Introduction	1
2. General EWDM and non-perturbative effect	2
3. Sommerfeld-Ramsauer-Townsend effect	4
3.1 Dependence on δm_+	5
3.2 Dependence on the EW interactions	5
3.3 Amplitudes of the wave functions	7
3.4 Dependence on DM velocity	8
3.5 Dependence on δm_N	9
4. Direct detection	10
5. Constraints from antiproton fluxes	11
6. PAMELA limit on various EWDM	13
6.1 Higgsino-like EWDM	13
6.2 Wino-like EWDM	14
6.3 Hyper-charged Triplet EWDM	15
7. Conclusions	17

1. Introduction

A multiplet of the Standard Model gauge group $SU(2)_L \times U(1)_Y$ [1] would be the simplest candidate of dark matter as it requires no additional ‘ad hoc’ interaction or couplings. Its electroweak interaction leads to a right thermal relic density if its mass is in the multi TeV range, and its stability is guaranteed automatically for a certain higher dimensional multiplet [2]. Another important feature of such an “Electro-Weak Dark Matter” (EWDM) is non-perturbative effects on its annihilation into gauge bosons which modifies significantly the tree-level results in the determination of its thermal relic density and its indirect detection rate [1, 3].

In this paper, we study such a non-perturbative correction for a Majorana or Dirac fermion EWDM in a wide range of its mass. That is, we will consider a “non-minimal” EWDM allowing an unspecified non-standard cosmology for the generation of a right relic density and a certain discrete symmetry for its stability. In the present Universe, the dark matter is highly non-relativistic and thus the wave-functions of the effective non-relativistic two-body EWDM states can get strongly modified by the non-abelian electroweak(EW)

potential in the process of their pair annihilation [1]. This is a generalization of the “Sommerfeld effect” [4] well-known for a single-component dark matter carrying an abelian gauge charge. Recall that the non-perturbative correction enhances (reduces) the annihilation cross section in case of an attractive (repulsive) Coulomb potential [3]. It will be interesting to note that an EWDM exhibits not only the usual Sommerfeld enhancement and resonance peaks but also a suppressed cross section for a certain choice of the parameters. This is a realization of the “Ramsauer-Townsend (RT) effect” [5] observed in low-energy electron scattering off gas atoms. We will show that such effects are caused mainly by the electromagnetic(EM) interaction in the two-body states of the charged components of an electroweak multiplet. An important feature is that the velocity distribution of dark matter particles has to be included in the non-perturbative calculation of the EWDM annihilation rate, as the “Sommerfeld-Ramsauer-Townsend” (SRT) resonance effect occurs when a certain condition is met among the model parameters, including the kinetic energy and so the speed of the annihilating states.

The non-perturbative correction to the EWDM annihilation cross section is important to set a limit on the EWDM, the most stringent constraints coming from the PAMELA measurement of the cosmic anti-proton flux [6, 7] and from the recent FERMI-LAT measurement of the diffuse gamma-ray emission in dwarf spheroidal galaxies [8]. In the present paper we will focus on the PAMELA antiproton limit, deriving a constraint which is a slightly stronger than the FERMI-LAT limit, and comparable to the result of Ref. [10] with the ‘MED’ propagation astrophysical parameters and a fixed secondary background.

In Section 2, we will give a general description of various electroweak multiplet dark matter candidates and present formulae to calculate the non-perturbative effect, summarizing the results in Refs. [1, 3]. Depending on whether the EWDM carries a hypercharge or not, it can be a Dirac or a Majorana fermion. In the first case, the neutral Dirac components have to split into two Majorana fermions with a mass gap sufficient to suppress the (inelastic) nucleonic scattering through the exchange of a Z boson. In Section 3, we discuss various features of the non-perturbative correction showing the SRT effect for the simplest example of a triplet EWDM with no hypercharge. Section 4 discusses values of the mass splitting which are large enough to avoid the current direct detection bound but still detectable in future experiments, depending on the dark matter mass. The antiproton yield from the EWDM annihilation to gauge bosons is analyzed in Section 5 to place a limit from the current cosmic antiproton flux measurements. We then calculate non-perturbative annihilation cross sections for various EWDM candidates to put a mass limit from the PAMELA data on the antiproton flux in Section 6. We conclude in Section 7.

2. General EWDM and non-perturbative effect

The dark matter particle can be the neutral component of an $SU(2)_L \times U(1)_Y$ fermion multiplet. As a specific example, we will consider a vector-like (Dirac) doublet with $Y = \pm 1/2$ (Higgsino-like), a (Majorana) triplet with $Y = 0$ (wino-like) and a vector-like (Dirac) triplet with $Y = \pm 1$. Note that a certain symmetry like Z_2 has to be imposed for the

stability of these EWDM candidates. Furthermore, the dark matter component of a Dirac multiplet is charged under $U(1)_Y$ and thus its scattering cross section with nuclei through Z boson exchange is far above the current limit from direct detection experiments. This constraint is however invalidated if there is a mass splitting in the Dirac dark matter fermion and thus the heavier Majorana fermion component cannot be excited by the nucleonic scattering of the lighter one (assumed to be the dark matter). A detailed analysis will be presented later to show that a mass splitting of order 0.2 MeV would be detectable while still allowed by the current data. Such a mass splitting can come from a higher dimensional operator between the EWDM and the Higgs doublet. For instance, the Higgsino-like dark matter multiplet, denoted by $\chi_u = (\chi^+, \chi^0)$ and $\chi_d = (\chi_d^0, \chi_d^-)$ in the chiral representation, allows the dimension-four operators:

$$\frac{1}{\Lambda}(H_u\chi_d)^2, \quad \frac{1}{\Lambda}(H_d\chi_u)^2, \quad \frac{1}{\Lambda}(H_u\chi_d)(H_d\chi_u), \quad (2.1)$$

where $H_u = (H^+, H^0)$ and $H_d = \epsilon H_u^*$ represent the Higgs doublets coupling to the up and down type quarks, respectively. Similarly, for the triplet EWDM multiplet with $Y = \pm 1$ consisting of two chiral fermions, $\chi_u = (\chi_u^{++}, \chi_u^+, \chi_u^0)$ and $\chi_d = (\chi_d^0, \chi_d^-, \chi_d^{--})$, the mass splitting between the Dirac pair $\chi_{u,d}^0$ can arise from:

$$\frac{1}{\Lambda^3}(H_u H_u \chi_d)^2, \quad \frac{1}{\Lambda^3}(H_d H_d \chi_u)^2, \quad \frac{1}{\Lambda^3}(H_u H_u \chi_d)(H_d H_d \chi_u). \quad (2.2)$$

On the other hand, the wino-like EWDM multiplet, a triplet with $Y = 0$ denoted by $\chi = (\chi^+, \chi^0, \chi^-)$ has only one Majorana neutral component. Note that a mass splitting between the charged and neutral components of order 0.1 GeV arises from the electroweak one-loop correction [2]. In the following sections, we will assume arbitrarily small mass gaps among the multiplet components which make a big impact on the non-perturbative annihilation rate of the EWDM particle.

In the non-relativistic pair annihilation of the EWDM, the non-perturbative effect due to the exchange of the electroweak gauge bosons mixes together the two-body states of the multiplet components. In the case of the Higgsino-like EWDM, there are three states formed by the charged (Dirac) component and two neutral (Majorana) components: $\chi_u^+ \chi_d^-$, $\chi_1^0 \chi_1^0$ and $\chi_0^0 \chi_0^0$, where χ_0^0 denotes the dark matter component. For the wino-like EWDM, we have two two-body states: $\chi^+ \chi^-$ and $\chi^0 \chi^0$. The triplet EWDM with $Y = \pm 1$ has four two-body states: $\chi_u^{++} \chi_d^{--}$, $\chi_u^+ \chi_d^-$, $\chi_1^0 \chi_1^0$ and $\chi_0^0 \chi_0^0$.

The Green's functions g_{ij} corresponding to the processes summarized above, where the indices i and j run over the two-body states of each EWDM candidate, verify the Schrödinger equation [1]:

$$-\frac{1}{m_{DM}} \frac{\partial^2 g_{ij}(r)}{\partial r^2} + V_{ik}(r) g_{kj}(r) = K g_{ij}(r), \quad (2.3)$$

with m_{DM} the mass of the dark matter particle, and the boundary condition $g_{ij}(0) = \delta_{ij}$ and $\partial g_{ij}(\infty)/\partial r = i\sqrt{m_{DM}(K - V_{ii}(\infty))} g_{ij}(\infty)$. Here $K = m_{DM}\beta^2$ is the total kinetic energy of the two initial dark matter particles in the annihilation process, where β is the

velocity of the DM particle in the frame of the galactic halo. Then, the dark matter pair annihilation cross section is given by:

$$\sigma v(\chi_0^0 \chi_0^0 \rightarrow AB) = 2d_{0i}d_{0j}^* \Gamma_{ij}^{AB}, \quad (2.4)$$

where $d_{0j} = g_{0j}(\infty)$ and $v = 2\beta$ is the relative velocity between the two incident DM particles. Here A, B run over the gauge bosons (W^+, W^-, Z, γ), that is, the gauge boson final states are $AB = (W^+W^-, ZZ, \gamma Z, \gamma\gamma)$. Taking the normalization of the covariant derivative $D_\mu = \partial_\mu + ig_2 A_\mu T^A$ for each gauge boson A , the potential matrix in Eq. (2.3) and the tree-level annihilation matrix Γ_{ij} are given by [3]:

$$V_{ij}(r) = 2\delta m_{i0} \delta_{ij} - \alpha_2 N_i N_j \sum_A [T_{ij}^A]^2 \frac{e^{-m_A r}}{r}, \quad (2.5)$$

where $\delta m_{i0} = m_{\chi_i} - m_{\chi_0}$, and:

$$\Gamma_{ij}^{AB} = \frac{\pi \alpha_2^2}{2(1 + \delta_{AB})m_{DM}^2} f(x_A, x_B) N_i N_j \{T^A, T^B\}_{ii} \{T^A, T^B\}_{jj}, \quad (2.6)$$

$$\text{where } f(x_A, x_B) \equiv \frac{(1 - \frac{x_A + x_B}{2})}{(1 - \frac{x_A + x_B}{4})^2} \sqrt{1 - \frac{x_A + x_B}{2} + \frac{(x_A - x_B)^2}{16}} \text{ with } x_A = \frac{m_A^2}{m_{DM}^2}.$$

Here the normalization factor N_i is 1 or $\sqrt{2}$ for the Dirac (charged) or Majorana (neutral) two-body state, respectively.

3. Sommerfeld-Ramsauer-Townsend effect

In this section, we present a detailed study of the non-perturbative effect on the EWDM annihilation cross section $\sigma v^{WW+ZZ} \equiv \sigma v^{WW} + \sigma v^{ZZ}$ including both final states W^+W^- and ZZ . The wino-like EWDM system has the smallest number of states and parameters: two bound states ($\chi^+\chi^-$ and $\chi^0\chi^0$) and one mass gap between them. For this reason, to simplify our discussion in this section we will focus on the example of wino-like dark matter, unless otherwise stated. As will be discussed in Section 5, EWDM can copiously produce W and Z bosons leading to a sizable contribution to the antiproton flux measured by cosmic-ray detection experiments such as PAMELA. This puts strong constraints on the masses of the EWDM particles, as will be analyzed in Section 6.

One of the key observations in this work is that the non-perturbative effect on the EWDM annihilation cross section includes not only the Sommerfeld effect [4] which induces both an overall enhancement of the cross section and resonance peaks for particular values of masses and couplings[1], but also a suppression or resonance dips. We will refer to this as the ‘‘Ramsauer-Townsend effect’’ in the DM annihilation processes. The Ramsauer-Townsend effect is a quantum mechanical phenomenon found in the scattering of electrons by noble gas atoms: the collision probability reaches a minimum when the electron kinetic energy take a certain value [5]. This is analogous to what happens to the transmission coefficient of a one-dimensional potential well, which is enhanced (corresponding to a vanishing reflection probability) when certain conditions are met between the kinetic energy

of the incident particle and the potential depth and width. A similar phenomenon can occur in the process of EWDM annihilation in presence of a non-perturbative electroweak potential. In order to see how such a Ramsauer-Townsend resonance arises in this system, we will perform a numerical analysis of the Schrödinger equation (2.3) by changing the mass gaps, the electromagnetic, W and Z potentials, and the velocity of the DM particle. In particular, the latter is an important factor which can drastically change the behavior of the resonance peaks and dips. For this reason, in Section 6 we will include in our calculation of the annihilation cross section a convolution over the Galactic velocity distribution of the impinging dark matter particles, in order to compare it to the experimental bound.

We mention here that a plot showing dips for particular values of masses and couplings in the annihilation cross section of Dark Matter particles interacting in a non-perturbative electroweak potential was presented in Ref. [3]. To our knowledge, this is the only instance where the Ramsauer-Townsend effect has been shown in the literature in the context of dark matter annihilation. However, the authors of Ref. [3] did not mention this effect in their discussion.

3.1 Dependence on δm_+

In the determination of the non-perturbative effects of EWDM annihilation, the splitting between the masses of the dark matter and charged states is a crucial factor, since it controls the transition of the DM state to a particle able to experience the long-range effect of the electromagnetic(EM) interaction. The wino-like EWDM has two states χ^\pm and χ^0 whose mass splitting is defined by $\delta m_+ \equiv m_{\chi^+} - m_{\chi^0}$. In Figure 1, we present the cross sections of the wino-like DM annihilation to the W^+W^- and ZZ final states σv^{WW+ZZ} , as a function of m_{DM} for the two representative values $\delta m_+ = 166$ and 15 MeV, where 166 MeV is the typical mass splitting arising from the EW one-loop correction [2]. The velocity of the EWDM is fixed to be the typical value of $v/c = 10^{-3}$. Our result with $\delta m_+ = 166$ MeV, which shows the Sommerfeld enhancement and a resonance peak within the mass range presented, is consistent with Ref. [1]. For the smaller mass gap, one finds that the peak positions shift to smaller m_{DM} and a dip appears that before was missing. In this latter case, the smaller mass gap allows an easier access to the charged state, inducing a stronger non-perturbative effect which activates the Ramsauer-Townsend suppression. Actually, in the next subsection we will confirm that the Ramsauer-Townsend dips appear mainly due to the electromagnetic interaction of the charged states.

3.2 Dependence on the EW interactions

In this subsection, we will modify the electroweak potentials in order to see how the SRT effect is affected. In Figure 2, we first plot the annihilation cross sections to W^+W^- and ZZ as a function of m_{DM} for $\delta m_+ = 15$ MeV with and without the EM interaction. Then in Figure 3, we display the annihilation cross section for the same parameters of the previous figure, but we vary the masses of the Z or W boson. In particular, in Figure 3(a) we take $m_Z \rightarrow n \cdot m_Z$ and in Figure 3(b) $m_W \rightarrow n \cdot m_W$, where in both cases $n = 1/3, 1$, and 3 .

Figure 2 shows that the dip disappears when the EM interaction is turned off, confirming the role played by the EM potential in the Ramsauer-Townsend effect when the

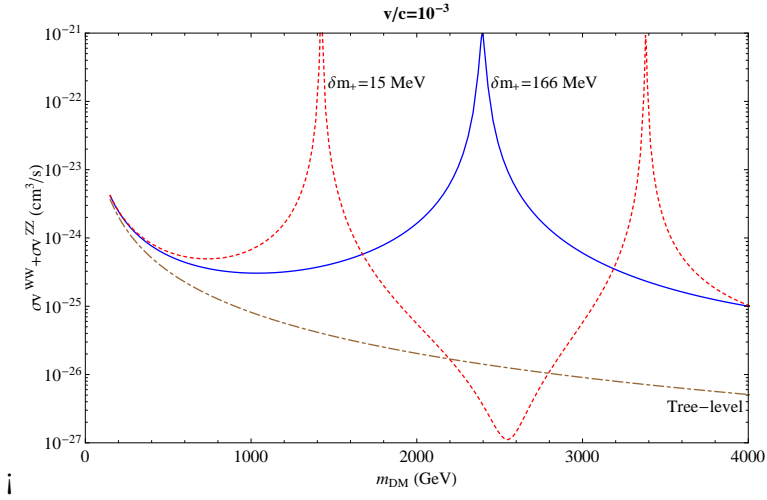


Figure 1: Annihilation cross sections of the wino-like EWDM for the mass splitting $\delta m_+ \equiv m_{\chi^+} - m_{\chi^0} = 166$ MeV (blue solid) and 15 MeV (red dotted). The brown dot-dashed line shows the tree-level cross section.

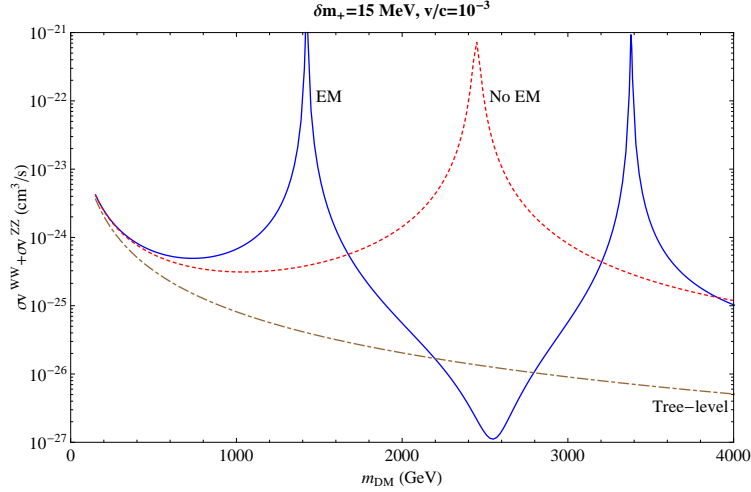


Figure 2: Annihilation cross sections for the wino-like EWDM with $\delta m_+ = 15$ MeV. The solid blue and red dotted lines show the results with and without the EM interaction, respectively. The brown dot-dashed line is the tree-level cross section.

mass gap between the dark matter and charged states is small. Furthermore, one finds that the behavior of the annihilation cross section without the EM interaction is almost the same as in Figure 1, where the influence of the EM interaction is blocked by a larger mass gap. This tells us that the SRT effect is insensitive to the mass gap as far as there is no long-range EM interaction.

The weak interaction via the Z or W boson exchange behaves like a long range interaction for a large DM mass, as can be seen in the large mass limit of Figures 1 and 2, where a sizeable SRT enhancement is present. A similar effect is expected to occur if smaller Z

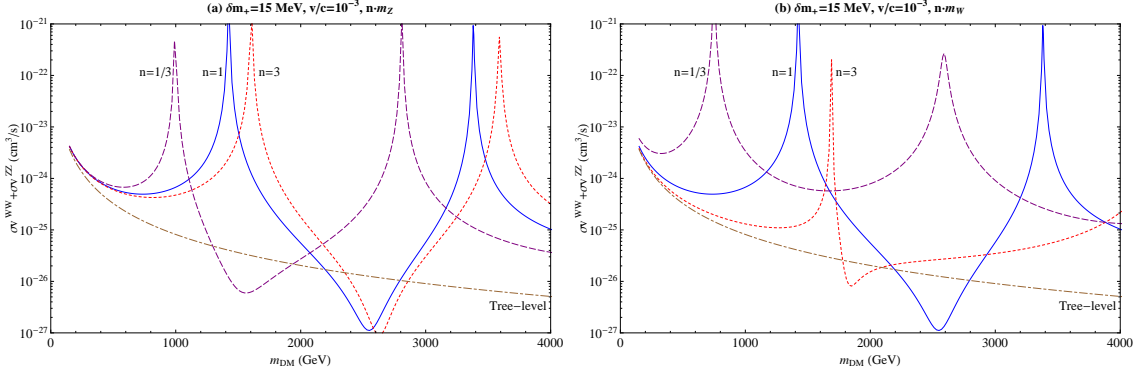


Figure 3: Annihilation cross sections for the wino-like EWDM with $\delta m_+ = 15$ MeV. Each panel shows the dependence on the interactions via the (a) Z and (b) W bosons. The purple dashed, blue solid, and red dotted lines respectively correspond to the cases of (a) $n \cdot m_Z$ and (b) $n \cdot m_W$ with $n = 1/3, 1$, and 3 . The brown dot-dashed line is the tree-level cross section.

or W boson masses are taken. However, this may change the resonance conditions for the SRT peaks and dips as well. As a consequence, Figure 3 shows that the peaks move to smaller values of the DM mass for smaller Z and W boson masses. Furthermore, one can find that the SRT effect is more sensitive to a change of the W boson mass compared to that of the Z boson mass. This can be explained by the fact that a change of the W boson mass influences not only the strength of the weak interaction via the W boson propagator, but also the accessibility thorough an EW charged current to a state able to interact electromagnetically. Moreover, Figure 3 (b) shows a drastic change in the Ramsauer-Townsend effect: in particular, the RT resonance condition cannot be met for a light W boson mass.

From the above discussion, it is also expected that the SRT peak and dip positions move to lighter DM masses as the electroweak interaction strength is increased. This is indeed what happens in the case of the quintuplet EWDM discussed in Ref. [3], which shows a RT dip at around $m_{DM} = 2$ TeV for a mass gap of order 100 MeV. On the other hand, no RT effect for such large values of the mass gap is observed for lower-dimensional EWDM and a dark matter mass within the multi-TeV range.

3.3 Amplitudes of the wave functions

As can be seen in Figures 1, 2, and 3, the annihilation cross sections of the EWDM show peaks and dips due to the SRT effect. To see their behavior in more detail, we present in Figure 4 the amplitudes of the wave functions d_{00} and d_{0+} connecting the two bound states $\chi^0 \chi^0$ and $\chi^+ \chi^-$ [see Eqs. (2.3) and (2.4)] of the wino-like EWDM with $\delta m_+ = 15$ MeV. One finds that each wave function has peaks and dips, implying both a constructive and a destructive resonance behavior. However, some difference is observed in the behavior of the peaks and dips. In particular, while peak positions coincide in the two wave function amplitudes, the dip positions do not. As a consequence, the dip in the annihilation cross section (the red-dotted line in Figure 1) appears between the two dips in the wave functions (the two lines in Figure 4) and is broader. However, the dip in the cross section can be

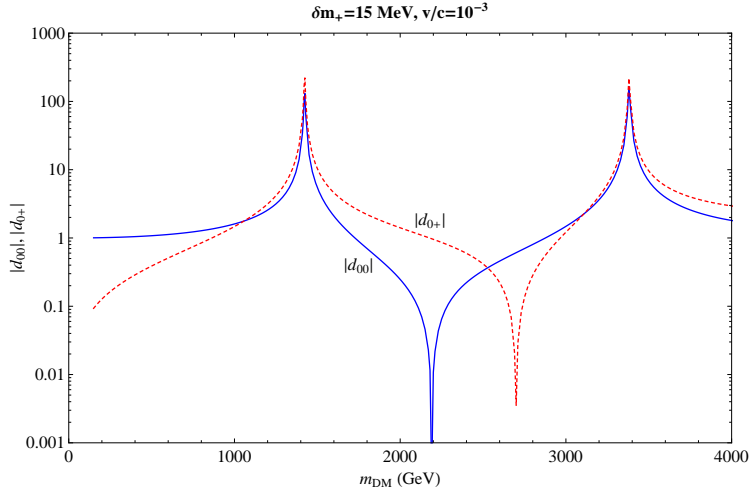


Figure 4: Wave function amplitudes for the two-body states of the wino-like EWDM with $\delta m_+ = 15$ MeV. The blue solid and red dotted lines show $|d_{00}|$ and $|d_{0+}|$, respectively.

more pronounced and even as narrow as in the case of Sommerfeld peaks in situations where the dips in the two wave functions are closer.

3.4 Dependence on DM velocity

As discussed in previous subsections, the SRT resonances occur when certain conditions are satisfied among the EWDM parameters such as the electroweak interaction strength, the mass gap and the kinetic energy (which depends on the DM velocity). So far, we fixed the DM velocity¹ to $v/c = 10^{-3}$. However, the DM particles in the halo of our Galaxy have a velocity distribution which is expected, for some particular values of the parameters, to smooth out the pattern of peaks and dips produced by the SRT effect. Therefore, for a real physical system it will be crucial to include the integration over the velocity distribution in the calculation the EWDM annihilation rate. In Figure 5, we present the values of σv^{WW+ZZ} in terms of the relative velocity v/c of the two DM particles for three representative values $m_{\text{DM}} = 1423, 2550$, and 3380 GeV, which correspond to the positions of the peaks and the dips of the red dotted line in Figure 1. As expected, the DM annihilation cross section shows a dependence on the velocity of the incoming DM particles. For the analysis of the PAMELA antiproton flux limit in Section 6, we will use the annihilation cross section obtained after velocity integration according to the following formula:

$$\langle \sigma v \rangle = N(v_{\text{esc}}) \int_0^{2v_{\text{esc}}} [\sigma v(v)] v^2 \exp \left[-\frac{3}{4} \left(\frac{v}{v_{\text{rms}}} \right)^2 \right] dv, \quad (3.1)$$

where $v_{\text{rms}} = 270$ km/s, $v_{\text{esc}} = 550$ km/s and $N(v_{\text{esc}})$ is the normalization constant.

¹This is also done in other analyses, for instance, in Refs. [1, 3].

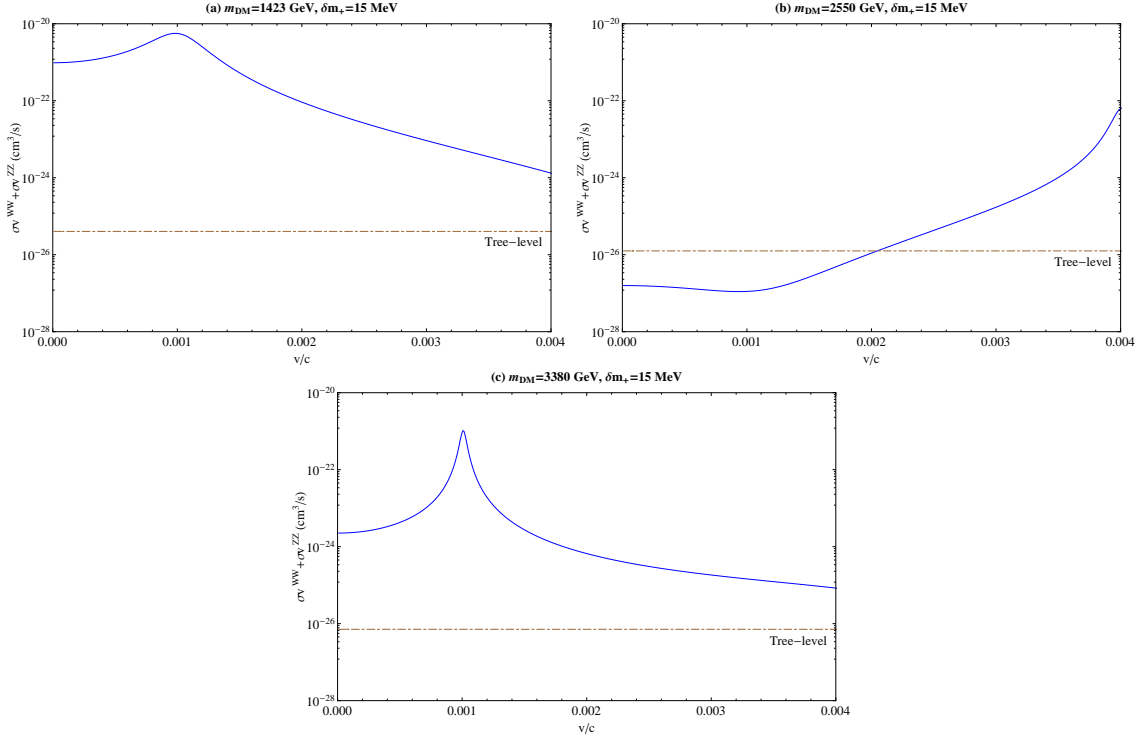


Figure 5: Annihilation cross sections for the wino-like EWDM with $\delta m_+ = 15$ MeV as functions of the relative velocity, v/c . For each panel, the used DM mass, m_{DM} , corresponds to the positions of the peaks and the dips of the red dotted line in Figure 1. The brown dot-dashed line is the tree-level cross section for each DM mass.

3.5 Dependence on δm_N

Before closing this section, we will check the dependence of the SRT effect on the mass splitting between the neutral states. The wino-like EWDM multiplet has only one Majorana neutral component, but, in general, EWDM multiplets can have more than one Majorana neutral component, whose masses are generically different from each other. In order to see the effect of the neutral mass splitting on the non-perturbative annihilation rate, we show σv^{WW+ZZ} for the Higgsino-like EWDM taking two values of the mass splitting: $\delta m_N \equiv m_{\chi_1^0} - m_{\chi_0^0} = 0.2$ and 200 MeV in Figure 6. Here the mass difference between the DM and charged states, $\delta m_+ \equiv m_{\chi^+} - m_{\chi_0^0}$, is fixed to be 341 MeV which is the typical mass splitting arising from the EW one-loop correction of Higgsino-like EWDM [2]. As one can see in Figure 6, the position of the peak is shifted from $m_{\text{DM}} \approx 8000$ GeV to $m_{\text{DM}} \approx 6800$ GeV when δm_N is changed from 200 MeV to 0.2 MeV. Note that in the previous Figure 1, the peak position moved from $m_{\text{DM}} \approx 2200$ GeV to $m_{\text{DM}} \approx 1200$ GeV when δm_+ was changed from 166 MeV to 15 MeV. Thus, one can conclude that the SRT effect for EWDM is much less sensitive to the neutral mass splitting compared to the splitting between the DM and charged states. In the following analysis, we will fix δm_N to 0.2 MeV (when applicable) corresponding to a situation for which direct detection is not excluded by the current experimental data and might yield a positive signal, as will be

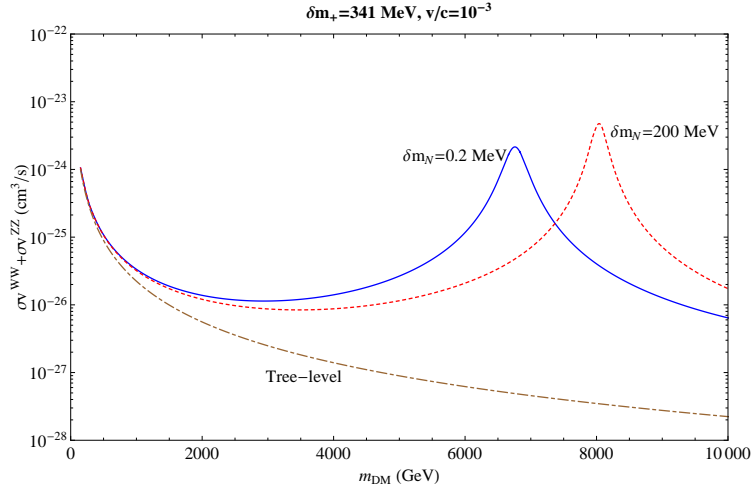


Figure 6: Annihilation cross sections for the Higgsino-like EWDM when $\delta m_N \equiv m_{\chi_1^0} - m_{\chi_0^0} = 0.2$ MeV (blue solid) and 200 MeV (red dotted). The mass difference between the charged and DM states, $\delta m_+ \equiv m_{\chi^+} - m_{\chi_0^0}$, is fixed as 341 MeV. The brown dot-dashed line shows the tree-level cross section.

shown in Section 4.

4. Direct detection

As already pointed out in Section 2, EWDMs with non-vanishing hypercharge Y have large couplings to nucleons driven by the exchange of a Z boson, so their elastic cross sections on nuclei is excluded by Dark Matter direct-detection experiments similarly to what typically happens for the simplest realizations of scenarios where the Dark Matter particle is a massive Dirac neutrino or a sneutrino. If, however, the elastic cross section for the EWDM is suppressed, inelastic scattering where the DM particle makes a transition to a slightly heavier neutral mass eigenstate is possible [11]. Notice that the wino-like EWDM has a vanishing hypercharge so is not subject to constraints from direct detection. In the case of the EWDM with $Y \neq 0$, the neutral (Dirac) component of the multiplet is split into two Majorana particles (the lightest of which is the DM particle), and thus the elastic cross section vanishes and only an inelastic transition of the DM particle to the heavier mass neutral state EWDM' is allowed. In particular, among the cases discussed in the previous sections, this scenario can be realized for the Higgsino-like EWDM ($T = 1/2$, $Y = \pm 1/2$) or for the triplet EWDM ($T = 1$) with $Y = \pm 1$.

The detection rate of inelastic scattering is suppressed by the relevant mass splitting δm_N . In particular, for a given recoil energy E_R there exists a minimal velocity for the dark matter β_{min} below which the kinetic energy is not sufficient to allow the transition to the excited state:

$$\beta_{min} = \sqrt{\frac{1}{2M_N E_R}} \left(\frac{M_N E_R}{\mu} + \delta m_N \right). \quad (4.1)$$

In the above equation M_N is the nuclear mass and μ is the reduced mass of the DM-particle and nucleus. Since the incoming velocity of DM particles is bounded from above by their escape velocity v_{esc} in the Galaxy while every DM direct detection experiment is able to detect DM scatterings only above a given lower-energy threshold E_{th} , detectable values of the parameter δm_N are bounded from above, typically a few hundreds keV depending on the target material and the energy threshold, while a comparison of the expected signals with the measured event rates allows to determine a lower bound on δm_N . Moreover, the EWDM-nucleon inelastic cross section by Z boson exchange is fully determined when the DM mass m_{DM} is fixed [2]:

$$\sigma_{EWDM,nucleon \rightarrow EWDM',nucleon} = c \frac{G_F^2 M_N^2}{2\pi} Y^2 (N - (1 - 4s_W^2)Z)^2, \quad (4.2)$$

where the mass splitting between the two neutral states is neglected, $c = 1$ for a fermionic EWDM, and Z and N are the number of protons and of neutrons in the target nucleus with mass M_N . This implies that the allowed range for δm_N can be plotted as a function of m_{DM} . This is done in Figure 7 for the case of the latest constraints from the XENON100 experiment [12]. In this figure, the solid lower curve refers to the case $Y = \pm 1$ while the dashed lower curve corresponds to $Y = \pm 1/2$. As explained above, values of δm_N above the upper curve are non-detectable, since in this case $c\beta_{min} > v_{max} = v_{esc} + v_{earth}$.² This is a purely kinematic constraint that does not depend on the EWDM-nucleus cross section, so the upper solid curve in the figure is common to the cases with $Y = \pm 1$ and $Y = \pm 1/2$. On the other hand, the lower curves represent the 90% C.L. lower bounds on δm_N obtained by applying Yellin's maximal gap procedure [13] to the spectrum (consisting of two nuclear recoil candidates at recoil energies 7.1 keV and 7.8 keV) detected by XENON100 in the range $6.6 \text{ keV} < E_r < 43.3$ [12]. In the calculation, we have assumed the standard value $\rho_{DM} = 0.3 \text{ GeV/cm}^3$ for the DM density in the neighborhood of the Sun and a Maxwellian velocity distribution truncated at $v_{esc} = 550 \text{ km/s}$ with $v_{rms} = 270 \text{ km/s}$.³

As it will be shown in detail, antiproton fluxes are almost insensitive to the particular choice of δm_N , while are very sensitive to the other mass splittings. Nevertheless, in the following sections we will fix $\delta m_N = 200 \text{ keV}$ (when applicable) corresponding to a situation for which direct detection is not excluded by present constraints and might yield a positive signal.

5. Constraints from antiproton fluxes

Since the EWDM is $SU(2)$ charged, their annihilations are expected to produce W/Z bosons copiously whenever this channel is kinematically allowed, leading to a sizeable

²Notice that β_{min} is defined in the detector rest frame, while v_{esc} is defined in the Galactic rest frame. For the Galilean boost we have assumed $v_{earth} = 232 \text{ km/s}$.

³In Ref. [12], the DM Region Of Interest (ROE) $6.6 \text{ keV} < E_r < 43.3$ is used when analyzing the data with a Profile Likelihood method, but is reduced to $6.6 \text{ keV} < E_r < 30.5 \text{ keV}$ when applying the maximum-gap method. While this does not imply a significant change in the limit for elastic scattering, the inelastic scattering bound is very sensitive to the upper bound of the ROI. For this reason, we derive our limit using the whole energy range of the XENON100 measurement.

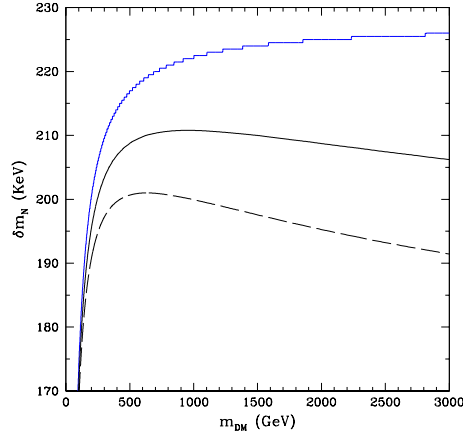


Figure 7: Values for the mass splitting δm_N which are detectable and experimentally allowed by the XENON100 direct detection experiment [12] as a function of the DM mass m_{DM} . The solid lower curve refers to the case $Y = 1$ and the dashed lower curve to the case $Y = 1/2$, while the solid upper does not depend on the value of the cross section and is common to both cases. When δm_N is above the upper curve the recoil energy is always below the XENON100 lowest-energy threshold $E_{th}=4$ keV. On the other hand, values below the lower curves are excluded at 90% C.L. by the 2 nuclear-recoil candidate events observed by XENON100 in the range $6.6 \text{ keV} < E_r < 43.3 \text{ keV}$ by applying Yellin’s maximal gap method [13].

primary contribution to the antiproton flux detected by experiments measuring cosmic-rays. The antiproton primary contribution from DM annihilation must be summed to the secondary antiproton contribution produced by energetic cosmic rays impinging on the interstellar medium. Although still affected by uncertainties, the latter contribution can be calculated in a relatively reliable way, and is in fair agreement to observation. This implies that no much room is left for the additional contribution from DM annihilation, and antiproton data can put constraints on the EWDM, namely on the EWDM annihilation cross section-times-velocity σv .

This is shown in Figure 8, where the circles represent the top-of-atmosphere antiproton flux as measured by PAMELA [7], while the dashed line is the secondary flux as calculated in Ref. [14], and rescaled by an overall factor 0.84. In this way, the model fits the data particularly well, with $\chi^2 = 12.1$ with 23 degrees of freedom. For this reason, we adopt this model as an estimation of the secondary flux. As far as the primary antiproton flux is concerned, we have used both the antiproton yields per annihilation and the propagation model according to Ref. [15], adopting for the latter an Einasto density profile with median values of the propagation parameters. Notice that, since the antiproton yields per annihilation corresponding to the two different final states WW and ZZ are practically undistinguishable, in the calculation of the expected signal the total cross section

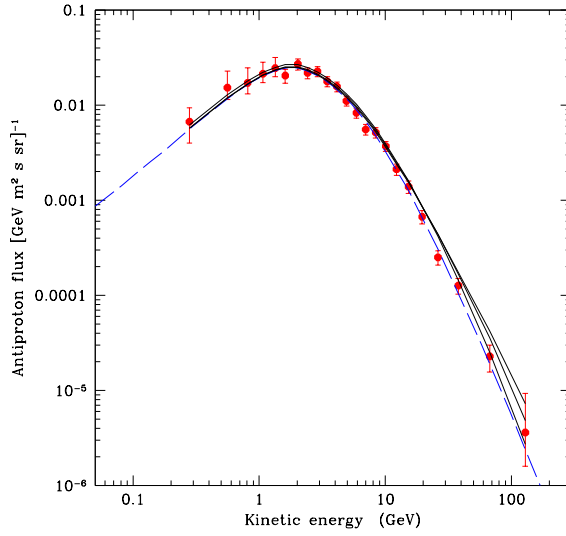


Figure 8: The circles show the antiproton top-of-atmosphere flux measured by PAMELA [7] as a function of the antiproton kinetic energy. The dashed line represents the secondary flux as calculated in [14] and rescaled by an overall factor 0.84. The solid lines show three expected fluxes from DM annihilation calculated as described in Section 5 for $m_{DM}=200$ GeV, 500 GeV, and 1 TeV, all corresponding to $\chi^2=44.2$.

$\sigma^{WW} + \sigma^{ZZ}$ is factorized.

The result of our analysis is shown in Figures 8 and 9. In particular, for each choice of m_{DM} and $\sigma v^{WW} + \sigma v^{ZZ}$ we sum the primary and secondary contributions of the expected antiproton flux and use the PAMELA data points to calculate a χ^2 , for which we assume an upper bound $\chi^2 < 44.2$, corresponding to the 99.5% C.L. with 23 degrees of freedom. In this way, we obtain the solid line shown in Figure 9. In Figure 8, the three solid lines show the expected antiproton flux for $m_{DM}=200$ GeV, 500 GeV and 1 TeV when $\sigma v^{WW} + \sigma v^{ZZ}$ lies on the boundary given in Figure 9.

6. PAMELA limit on various EWDM

As shown in Section 5, W and Z bosons produced by the annihilations of EWDMs provide a sizable contribution to the cosmic ray antiproton flux measured by PAMELA. Thus, for various EWDM models we will examine the DM mass ranges satisfying the PAMELA antiproton flux bound on σv^{WW+ZZ} as obtained in Section 5. As explained in Section 3.4, the annihilation cross section of the EWDM shows a DM velocity dependence. In this section, we will therefore calculate the annihilation cross section considering the velocity integration effect, and also, for comparison, present the result with a fixed velocity, $v/c = 10^{-3}$.

6.1 Higgsino-like EWDM

We first show the results for the Higgsino-like (doublet with $Y = \pm 1/2$) EWDM which is the smallest multiplet. In Figure 10, we present the annihilation cross sections (blue solid

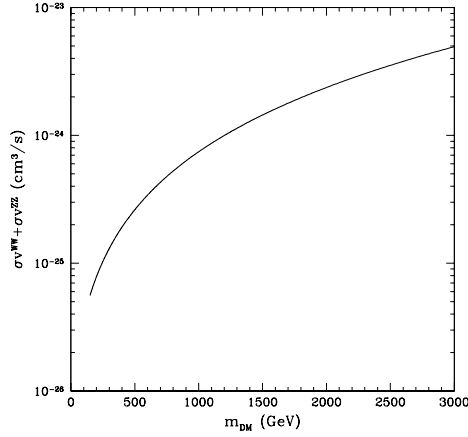


Figure 9: Estimation of the 99.5 % C.L. upper bound on the annihilation cross section times velocity $\langle\sigma v\rangle$ as a function of the DM mass m_{DM} . The values of $\langle\sigma v\rangle$ above the solid line have $\chi^2 > 44.2$ with 23 degrees of freedom when compared to the PAMELA data [7].

lines) for two representative values $\delta m_+ = 341$ and 8 MeV as a functions of m_{DM} , where the velocity integration effect is included. For comparison, we also show our results for a fixed relative DM velocity $v/c = 10^{-3}$ (red dotted lines). As already explained, in this plot and in the following ones the neutral mass splitting δm_N is taken to be 0.2 MeV, when applicable. For the higher mass splitting $\delta m_+ = 341$ MeV (a), we extended the DM mass range up to 10 TeV to see the first Sommerfeld peak. If we further extended the mass range, Ramsauer-Townsend dips would appear as well. On the other hand, for the smaller mass gap $\delta m_+ = 8$ MeV (b), the SRT resonances appear in the smaller DM mass range as discussed in Section 3.

As shown in the figures, the velocity integration smooths out the peaks and dips and changes the positions of the peaks in (b). With only the tree-level cross section, the region $m_{\text{DM}} \lesssim 364$ GeV is ruled out by the current PAMELA data. However, the annihilation cross section is enhanced by the SRT and consequently the excluded region is a bit extended to $m_{\text{DM}} \lesssim 382$ GeV in the case of the typical charged mass splitting for the Higgsino-like EWDM, $\delta m_+ = 341$ MeV [2]. In the case of a smaller mass splitting, the PAMELA limit can constrain also small bands around the Sommerfeld peaks, in addition to the low mass region, as can be seen in Figure 10 (b).

6.2 Wino-like EWDM

Figure 11 shows the annihilation cross sections for the wino-like (triplet with $Y = 0$) EWDM in the same way as in the Higgsino-like EWDM case. The two values $\delta m_+ = 166$ and 6 MeV are taken for the analysis, in order to show the dependence on the charged mass splitting. One can see from Figure 11 that the velocity integration makes a big change in

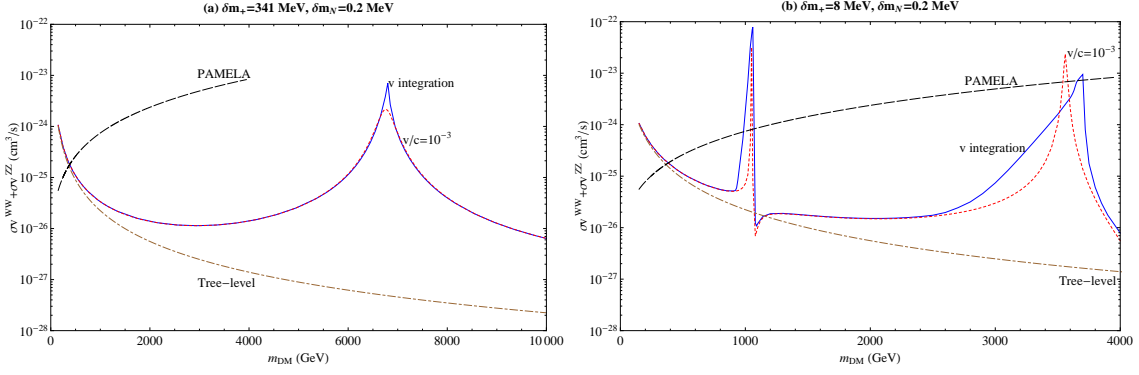


Figure 10: Annihilation cross sections to W^+W^- and ZZ for the Higgsino-like EWDM with $\delta m_+ =$ (a) 341 MeV and (b) 8 MeV, and $\delta m_N = 0.2$ MeV. In each panel, the blue solid line is our final result obtained after velocity integration, while the red dotted line is the cross section with the fixed velocity, $v/c = 10^{-3}$. The black long-dashed line shows the upper limit obtained from the PAMELA antiproton flux data analysis in Section 5. The brown dot-dashed line is the tree-level cross section.

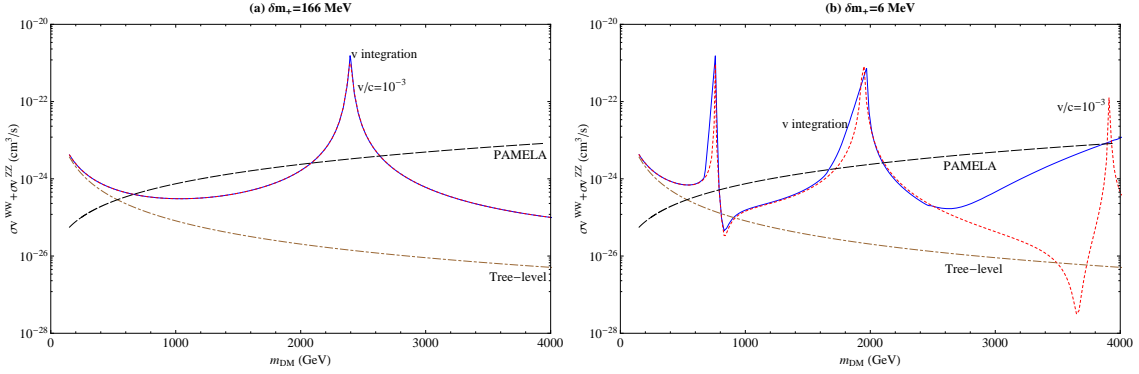


Figure 11: Annihilation cross sections to W^+W^- and ZZ for the wino-like EWDM when $\delta m_+ =$ (a) 166 MeV and (b) 6 MeV. Each line represents the same thing as in Figure 10.

the case of the smaller mass gap, erasing out some of the peaks and dips in 11 (b). While the tree-level result excludes the mass range $m_{\text{DM}} \lesssim 533$ GeV, the non-perturbative effect extends the constrained region up to $m_{\text{DM}} \approx 664$ GeV for the representative charged mass splitting of the wino-like EWDM, $\delta m_+ = 166$ MeV[2]. For the smaller mass gap $\delta m_+ = 6$ MeV the PAMELA limit gets stronger, excluding DM masses below 900 GeV and also bands around the peaks which are larger compared to the Higgsino-like EWDM case.

6.3 Hyper-charged Triplet EWDM

Now let us consider a more complicated case, the triplet EWDM with $Y = \pm 1$ which has one doubly charged, one singly charged, and two neutral components. Thus, the DM component χ_0^0 can have three mass splittings: $\delta m_{++} \equiv m_{\chi^{++}} - m_{\chi_0^0}$, $\delta m_+ \equiv m_{\chi^+} - m_{\chi_0^0}$, and $\delta m_N \equiv m_{\chi_1^0} - m_{\chi_0^0}$. Figure 12 presents the annihilation cross sections for $(\delta m_{++}, \delta m_+) =$

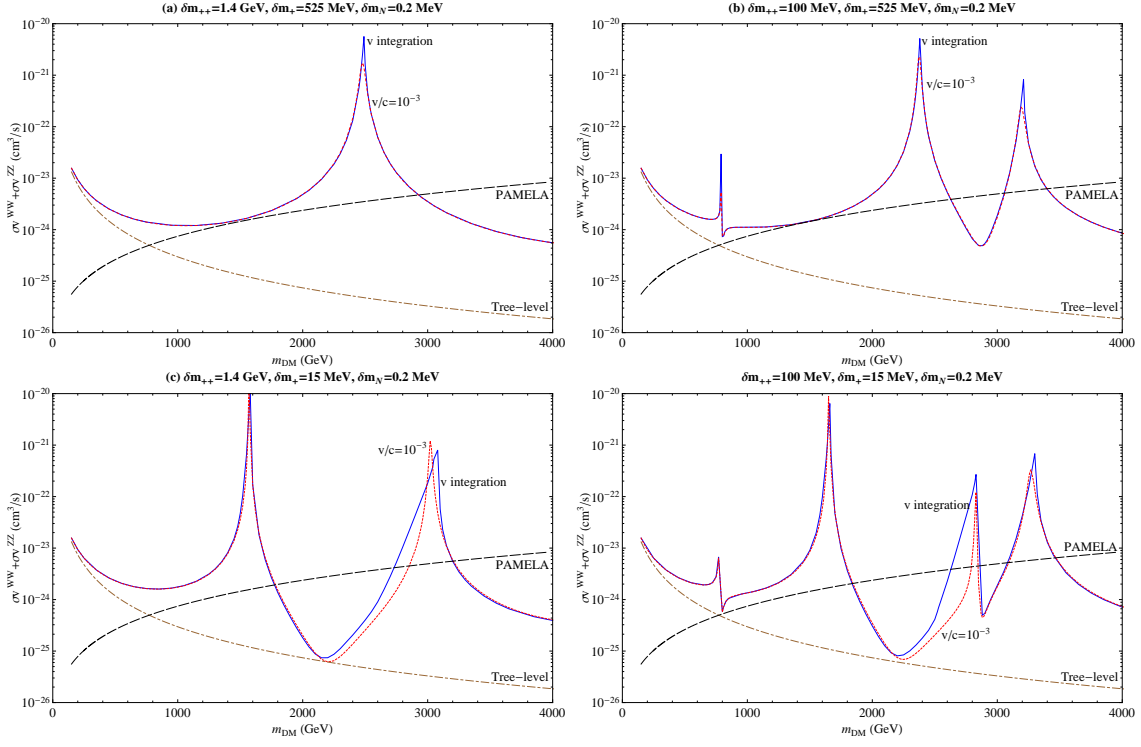


Figure 12: Annihilation cross sections to W^+W^- and ZZ for the triplet EWDM with $Y = \pm 1$. The used values of $\delta m_{++}, \delta m_+, \delta m_N$ are shown in each panel. Each line represents the same thing as in Figure 10.

(1400, 525), (100, 525), (1400, 15), and (100, 15) MeV fixing $\delta m_N = 0.2$ MeV. Note that $\delta m_{++} = 1400$ MeV and $\delta m_+ = 525$ MeV correspond to the typical mass splittings due to the EW one-loop corrections [2].

One can see the dependence of the SRT effect on the doubly charged mass splitting δm_{++} comparing the two cases $(\delta m_{++}, \delta m_+) = (1400, 525)$ and $(100, 525)$ MeV in Figures 12 (a) and (b), while the dependence on the singly charged mass splitting δm_+ can be understood comparing the two cases $(\delta m_{++}, \delta m_+) = (1400, 525)$ and $(1400, 15)$ MeV in Figures 12 (a) and (c). In particular, one can see that a larger number of peaks and dips appears when δm_{++} is reduced by a factor 14 compared to the case when δm_+ is reduced by a factor 35. This shows that the SRT effect is more sensitive to δm_{++} than to δm_+ due to the stronger EM interaction of multiply-charged states. In addition, Figure 12 (d) shows the combined effect of the changes of δm_{++} and δm_+ shown separately in Figures 12 (b) and (c). The hyper-charged triplet EWDM has stronger EW interactions compared to the Higgsino-like or wino-like EWDM and thus exhibits a stronger SRT effect. As a consequence, the excluded mass region reaches about 3 TeV for the typical mass gaps of $\delta m_{++} = 1400$ MeV and $\delta m_+ = 525$ MeV, while the tree-level limit is as low as about 800 GeV as shown in Figure 12 (a). It is interesting to see that regions of small DM mass are allowed for smaller mass gaps, as shown in Figures 12 (b,c,d) due to the RT effect. One would expect to find more regions of lower DM mass allowed for lower mass gaps.

7. Conclusions

In the present paper, we have discussed the non-perturbative effects occurring in the annihilation cross section of an “Electro-Weak Dark Matter” (EWDM) particle belonging to an $SU(2)_L \times U(1)_Y$ multiplet, when the splittings between the DM state mass and that of the other charged or neutral component(s) of the multiplet are treated as free parameters. In particular, we have considered a vector-like (Dirac) doublet with $Y = \pm 1/2$ (Higgsino-like), a (Majorana) triplet with $Y = 0$ (wino-like) and a vector-like (Dirac) triplet with $Y = \pm 1$. In all these examples, an ad hoc symmetry has to be imposed for the stability of EWDM, and we have allowed for an unspecified non-standard cosmology for the generation of the right dark matter relic density, since the thermal abundance of EWDM is typically below that required by observation unless its mass is in the multi-TeV range. Moreover, in the case of EWDM charged under $U(1)_Y$, severe constraints from direct detection searches exist on the elastic cross section off nuclei. However, these limits can be circumvented in presence of a sufficiently large mass splitting (of the order of 0.2 MeV) in the Dirac dark matter fermion, so that only inelastic scattering is allowed and kinematically suppressed.

As a result of our analysis, it is shown that EWDM exhibits not only the usual Sommerfeld enhancement of the cross section with resonance peaks at particular values of the dark matter mass, but also a suppressed cross section for particular choices of the parameters. The latter phenomenon is a realization of the “Ramsauer-Townsend effect” observed in low-energy electron scattering off gas atoms. Moreover, we have shown that the EWDM mass for which non-perturbative effects become important is particularly sensitive to the mass splittings between the dark matter and the charged components of the EW multiplet, and is driven below the TeV scale when this mass splitting is reduced to a few MeV. In particular, we have shown that when the mass splitting gets smaller the transition of the dark matter particles to electrically charged states is made easier, and it is the electromagnetic long-range interaction between these charged states which is responsible both of the Sommerfeld enhancement of the cross section and of the Ramsauer-Townsend suppression, even when the dark matter mass is not much larger than the EW gauge boson masses. Notice that only mass splittings larger than 100 MeV, induced by EW radiative corrections, have been considered so far in the literature, so that, before our analysis, the Sommerfeld effect had been discussed only in the context of multi-TeV scale dark matter.

Based on the results explained above, we have then used available experimental constraints on the exotic component of the antiproton flux in cosmic rays to put constraints to the EWDM parameter space. Since non-perturbative effects depend on the velocity of the dark matter particles, we have calculated the annihilation cross section considering the effect of the convolution of the cross section with the velocity distribution of the dark matter particles in the Galaxy, showing that in some cases this can smear out or significantly modify the pattern of Sommerfeld-Ramsauer-Townsend peaks and dips obtained for a fixed value of the velocity. Typically, we have found constraints on the EWDM mass ranging between a few hundred GeV to a few TeV, depending on the specific EWDM realization and on the values of the mass splittings. However, we have also found that, by an appropriate choice of the mass splittings, sometimes the Ramsauer-Townsend suppression in

the annihilation cross section can allow to recover narrow intervals at lower values of the EWDM mass.

Finally, in the case of EWDM charged under $U(1)_Y$ we have found that the phenomenology described above is not particularly sensitive to the mass splitting between the two neutral Majorana states. As a consequence, this mass difference can be chosen so that the inelastic cross section of the EWDM off nuclei is allowed by present direct detection constraints and at the same time is within the reach of future experiments.

Acknowledgments

S.S. acknowledges support by the National Research Foundation of Korea (NRF) with a grant funded by the Korea government (MEST) no. 2011-0024836.

References

- [1] J. Hisano, S. Matsumoto and M. M. Nojiri, Phys. Rev. Lett. **92** (2004) 031303 [hep-ph/0307216]. J. Hisano, S. Matsumoto, M. M. Nojiri and O. Saito, Phys. Rev. D **71** (2005) 063528 [hep-ph/0412403].
- [2] M. Cirelli, N. Fornengo and A. Strumia, Nucl. Phys. B **753**, 178 (2006) [hep-ph/0512090].
- [3] M. Cirelli, A. Strumia and M. Tamburini, Nucl. Phys. B **787** (2007) 152 [arXiv:0706.4071 [hep-ph]].
- [4] A. Sommerfeld, Annalen der Physik, 403, 257 (1931).
- [5] C. W. Ramsauer, Ann. Phys. (Leipzig) 64, 513 (1921); 66, 545 (1921); J. S. Townsend and V. A. Bailey, Philos. Mag. 43, 593 (1922); N. F. Mott and H. S. W. Massey, The Theory of Atomic Collisions (Oxford Univ. Press, Oxford, 1933).
- [6] O. Adriani, G. C. Barbarino, G. A. Bazilevskaia, R. Bellotti, M. Boezio, E. A. Bogomolov, L. Bonechi and M. Bongi *et al.*, Phys. Rev. Lett. **102**, 051101 (2009) [arXiv:0810.4994 [astro-ph]].
- [7] O. Adriani *et al.* [PAMELA Collaboration], Phys. Rev. Lett. **105**, 121101 (2010) [arXiv:1007.0821 [astro-ph.HE]].
- [8] M. Ackermann *et al.* [Fermi-LAT Collaboration], Phys. Rev. Lett. **107** (2011) 241302 [arXiv:1108.3546 [astro-ph.HE]].
- [9] E. J. Chun, JHEP **0912** (2009) 055 [arXiv:0909.3408 [hep-ph]].
- [10] G. Belanger, C. Boehm, M. Cirelli, J. Da Silva and A. Pukhov, arXiv:1208.5009 [hep-ph].
- [11] D. Tucker-Smith and N. Weiner, Phys. Rev. D **64**, 043502 (2001) [hep-ph/0101138].
- [12] E. Aprile *et al.* [XENON100 Collaboration], arXiv:1207.5988 [astro-ph.CO].
- [13] S. Yellin, Phys. Rev. D **66**, 032005 (2002) [physics/0203002].
- [14] V. S. Ptuskin, I. V. Moskalenko, F. C. Jones, A. W. Strong and V. N. Zirakashvili, Astrophys. J. **642** (2006) 902 [astro-ph/0510335].
- [15] M. Cirelli, G. Corcella, A. Hektor, G. Hutsi, M. Kadastik, P. Panci, M. Raidal and F. Sala *et al.*, JCAP **1103**, 051 (2011) [arXiv:1012.4515 [hep-ph]].